Experimental and analytical study on steel-concrete-ECC composite frames with URSP-S connectors

Linli Duan[a,b], Xin Nie[a*], Jiaji Wang[c] and Gaoqiao Wu[a]

[a] Key Laboratory of Civil Engineering Safety and Durability of China Education Ministry, Department of Civil Engineering, Tsinghua University, Beijing 100084, China

[b] School of Civil Engineering, Central South University, Changsha 410075, China

[c] Department of Civil Engineering, The University of Hong Kong, Hong Kong 999077, China

Abstract: To improve the slab crack resistance in the hogging moment region of steel-concrete composite frames, this paper proposes using Engineered Cementitious Composite (ECC) and Uplift-Restricted and Slip-Permitted Screw-type (URSP-S) connectors near the columns of the frames, the structural behavior of the innovative steel-concrete-ECC composite frames were experimentally and numerically investigated. Firstly, five 1/2-scaled steel-concrete composite frames were experimentally studied under vertical uniform slab loading and horizontal low cyclic loading. The failure mode and cracking, load-displacement relationship, stiffness and strength degradation, energy dissipating, and strain of composite frames with ECC and URSP-S connectors were analyzed, and good cooperative behavior and overall seismic performance were found. Then, it was compared with the results of the other four specimens with different slab materials and shear connector types. The experimental results showed that the use of ECC and URSP-S connectors improved slab crack resistance 55% in terms of crack width, and rarely influenced the structural performance of the composite frames. ECC played a major role in controlling the crack width while URSP-S connector played a major role in controlling the crack number.

* Corresponding author. E-mail: xinnie@tsinghua.edu.cn (X. Nie)

In addition, based on the test specimen with ECC and URSP-S connectors, an elaborate finite element (FE) model was developed and validated by the test results in terms of cyclic curves and failure mode. Moreover, supplementary modeling analyses with various parameters on the influence of the frame capacity were performed, where steel beam height was the most influential parameter.

Keywords: Steel-concrete composite frame; Engineered Cementitious Composite (ECC); Uplift-Restricted and Slip-Permitted Screw-type (URSP-S) connector; Seismic behavior; Crack

1. Introduction

Since the steel-concrete composite frames take full advantage of the characteristics of steel and concrete, it has excellent mechanical properties and natural assembly advantages, providing a high-performance and sustainable structural form for the green and rapid construction of building projects [1-3]. The concrete slab has both positive and negative impacts on the steel-concrete composite frames. The spatial composite effect of the concrete slab enhances the capacity and stiffness of the frames [4]. However, the cracking control of the concrete slab under hogging moment becomes a crucial problem. It significantly influences the performance of the structure, including strength, stiffness and durability [5, 6], especially for complex structures with large spans and under severe loads or extreme environmental conditions. Therefore, efficient and reasonable control measures are urgently needed to meet the demand for crack control in the hogging moment region of steel-concrete composite structures.

The use of innovative materials is one of the effective ways to meliorate crack resistance of structural components. Engineered Cementitious Composites (ECC), proposed by Victor Li [7] according to micromechanics and fracture mechanics, possess high tensile ductility, strain-hardening and multiple-cracking in tension, while directly softening after cracking for normal concrete (see Fig. 1(a)). The crack width of ECC due to tensile force is generally less than 100 microns [8, 9], and ECC was effective in delaying propagation of cracks [10, 11]. Due to the unique properties, many researchers have gradually applied ECC to the steel-concrete composite beams [12, 13], composite columns [14], composite steel plate shear walls [15] and composite frames [16]. The application of ECC has been proved to achieve an excellent crack resistance effect and improve the structural performance of the structure under monotonic and low cyclic loading.

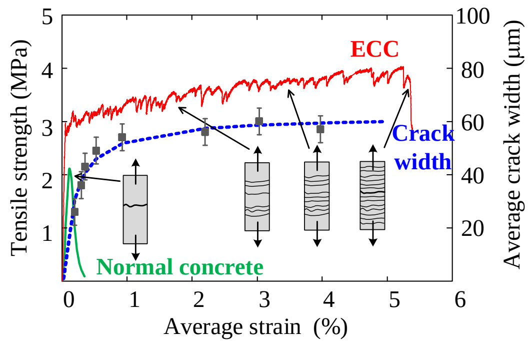

(a) ECC properties [8]

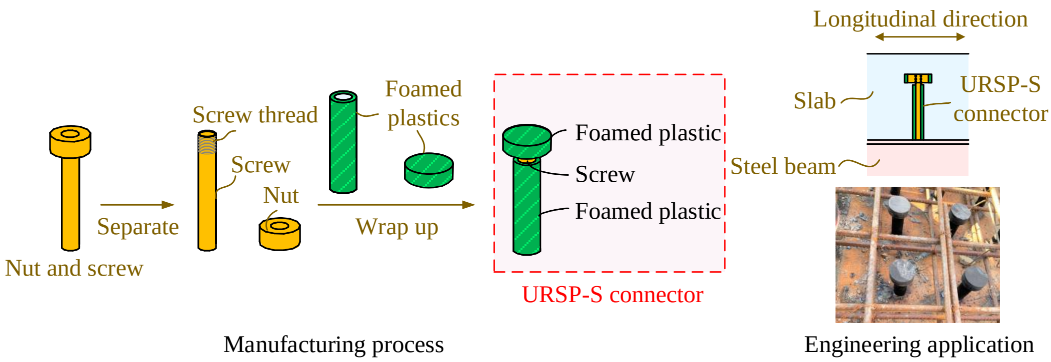

(b) URSP-S connectors

Fig. 1. ECC and URSP-S connectors.

The Uplift-Restricted and Slip-Permitted Screw-type (URSP-S) connector is a new type of connector invented by Nie [17] to address the cracking problem. By wrapping with a low elastic modulus material around screw and nut (see Fig. 1(b)), the URSP-S connectors can release their shear resistance of interface to a certain extent in the longitudinal direction while resisting the vertical separation between concrete and steel. Therefore, the tensile stress of the concrete slab and the risk of cracking were reduced [17]. In recent years, some theoretical, experimental and numerical researches have been completed on the URSP-S connectors at the level of components and systems. The theoretical mechanism of the steel-concrete composite beams arranged with this new type of connectors was explored [18], experiments on steel-concrete composite beams [19], curved composite beams [20], composite frames [21] with URSP-S connectors were carried out, and numerical analysis on the composite frame joint with the consideration of constitutive model of URSP-S connectors was conducted [22], design guidelines and construction suggestion in a continuous composite bridge were also proposed [23]. The investigations and applications of URSP-S connectors in the composite structure were proved to achieve a good crack resistance effect and possess a simple construction and convenient material in engineering applications.

Despite the advantage of crack resistance improvement of ECC and URSP-S connectors, few studies have focused on the steel-concrete composite frame with ECC and URSP-S connectors. Moreover, the structural behavior of the composite frame needs to be explored. Therefore, for this study, it is of interest to investigate the feasibility of applying ECC and URSP-S connectors together near columns in steel-concrete composite frame structures. The frame specimen with both ECC and URSP-S connectors with a 1/2 scale was conducted under vertical and lateral loading, the failure modes and hysteretic behaviour of the frame were revealed and compared with the results of the other four specimens with various slab materials and shear connectors. Finiteelement simulation of the steel-concrete-ECC composite frame with URSP-S connectors in MSC. Marc [24] was explored, which were validated by the test results and further conducted under various parameter analyses. The results obtained from this study will promote the use of ECC and URSP-S connectors of composite frames on improving the structural performance under hogging moment.

2. Experimentation

2.1 Specimen details

The test specimen was extracted from a high-rise prototype structure based on inflection point and symmetry [21], and a large scale of 1/2 was used. Five frame specimens, consisting of rectangular concrete-filled steel tubular (CFST) column and steel-concrete/ECC composite beam with URSP-S/studs shear connectors, were designed and experimented under various loads. As listed in Table 1, the test specimens include one specimen with conventional stud and concrete (abbreviated as SC), two specimens with different lengths of URSP-S connectors (abbreviated as SCU, SCU2) and one specimen with ECC (abbreviated as SCE) arranged near the column, which have been reported by the authors [16, 21], and one specimen with both URSP-S connectors and ECC (abbreviated as SCUE) reported in this paper, whose structural configuration is detailed in Fig. 2.

Table 1 Details of the five test specimens.

Specimens	Material of Slab	Connectors in composite beams	Reported in
SC	Concrete	Studs	
SCU	Concrete	URSP-S connectors (near columns)+ studs	Ref. [21]
SCU2	Concrete	URSP-S connectors	
SCE	ECC (near columns)+Concrete	Studs	Ref. [16]
SCUE	ECC (near columns)+Concrete	URSP-S connectors (near columns)+ studs	This paper

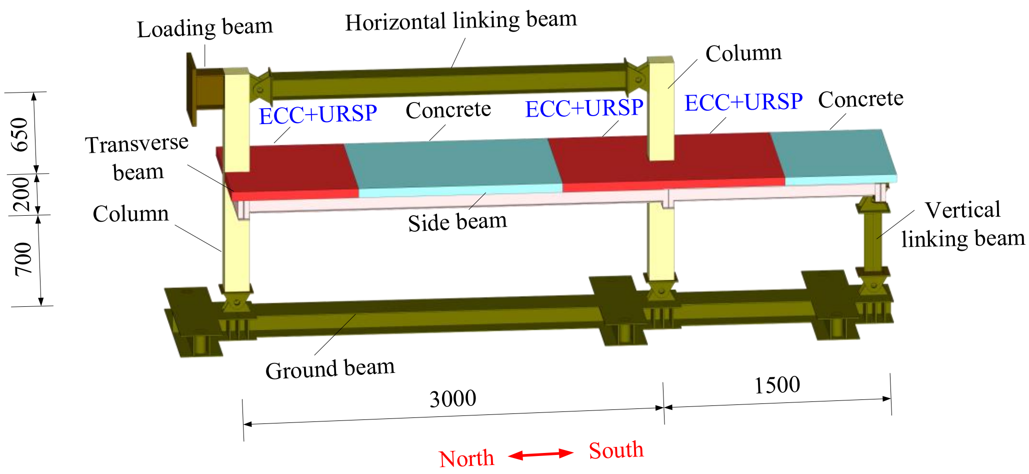

(a) General view

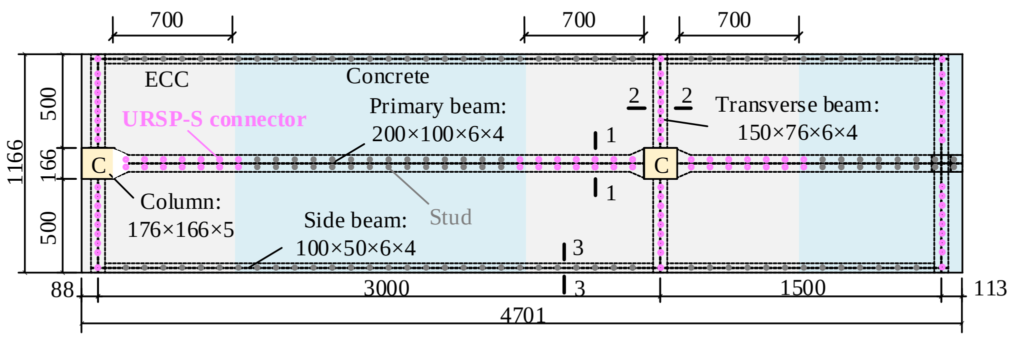

(b) Detailed dimensions and configurations

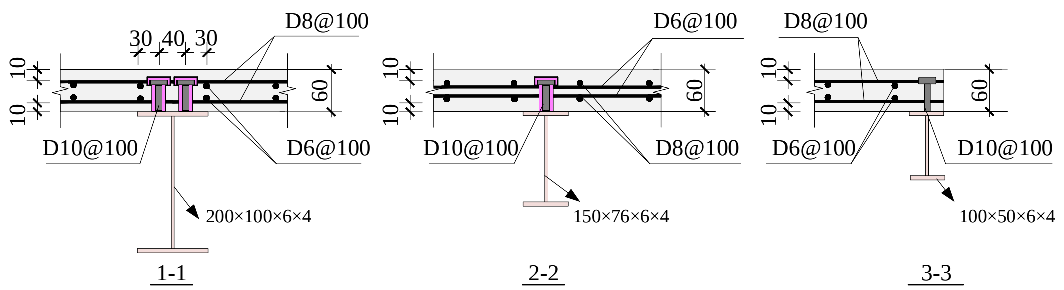

(c) Sectional configurations

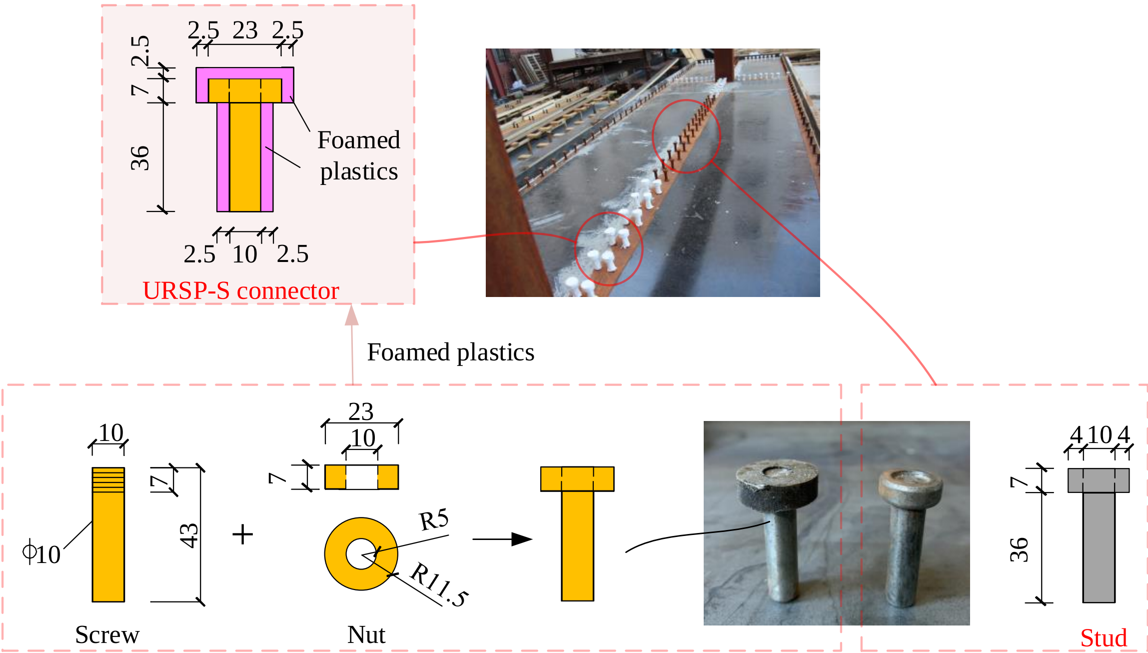

(d) Stud and URSP-S connector

Fig. 2. The structural configuration of test Specimen SCUE (in units of mm).

Fig. 2(a) gives the overview of the Specimen SCUE, whose length was 4500 mm and the height was 1550 mm. The design of the specimen follows the requirements of the Chinese codes JGJ 138-2016 and GB 50011-2010 [25, 26]. The slab had a width of 1166 mm and a thickness of 60 mm. CFST column had a dimension of 176×166×5 mm (length×width×thickness), and 200×100×6×4 mm (height×width×flange thickness×web thickness) for the primary steel beam, as depicted in Fig. 2(b). The composite joints adopted the diagram-through joints, which were proved to perform well according to the previous study [21]. Three key sectional configurations of composite beams are given in Fig. 2(c). The diameters of longitudinal and transverse rebar were 6 mm and 8 mm, respectively, and were employed with double layers in the slab. The spacings of the reinforcements were 100 mm. Fig. 2(c) and (d) show the detailed arrangement and dimensions of shear connectors, respectively. The design of the nut and the foamed plastics of URSP-S connectors follow the uplift requirement and the recommendation in Ref. [19, 21]. The design of the conventional studs and screw of URSP-S connectors were same [21]. To provide full composite action of the composite beam, the size was 43×10 mm (height×diameter), two and a single row of connectors with a spacing of 100 mm were adopted on the primary steel beam and secondary steel beams, respectively.

2.2 Material properties

The material properties of concrete and ECC were shown in Table 2, which were obtained by the material tests concurrently as the loading of the frame specimens. The compressive strengths of concrete and ECC were tested as per GB/T 50081-2019 [27], the tensile test of ECC with dog-bone specimens reported in Ref. [16, 28] was adopted in this study. A typical tensile stress–strain curve of ECC in the test is illustrated in Fig. 3(a). In addition, the mix proportions of ECC used in the test are given in Table 3. The PVA fiber used in ECC had a density of 1.2 g/cm^3, a tensile strength of 1620 MPa and an elastic modulus of 42.8 GPa. The diameter of PVA fiber was 0.039 mm and the length was 12 mm. Table 4 gives the mechanical properties of steel plates and rebar as per GB/T228-2010 [29]. A typical tensile stress–strain curve of steel plate in the test is show in Fig. 3(b).

Table 2 Mechanical properties of concrete and ECC.

Material	Strength grade	f_c (MPa)	f_t (MPa)	ε
Concrete (slab)	C30	43.7	/	/
Concrete (column)	C40	48.4	/	/
ECC	/	57.1	1.8	0.6%

Note: f_c represents the cylindrical compressive strength; f_t and ε represent ultimate tensile strength and strain, respectively.

Table 3 Mix proportions of 1 m^3 ECC.

Ingredient	Cement	Superplasticizer	Sand	Water	Silica fume	Fly ash	Fiber	Expansive agent
Weight (kg)	782.5	6	360	420	60	240	20.4	120

Table 4 Mechanical properties of steel.

Type of steel	Strength grade	Thickness/Diameter (mm)	f_y (MPa)	f_u (MPa)
Steel plate	Q345	4	359	475
		5	376	521
		6	402	546
Reinforcement	HPB300	6	440	598
	HRB400	8	439	695

Note: f_y and f_u represent yielding and ultimate strength, respectively.

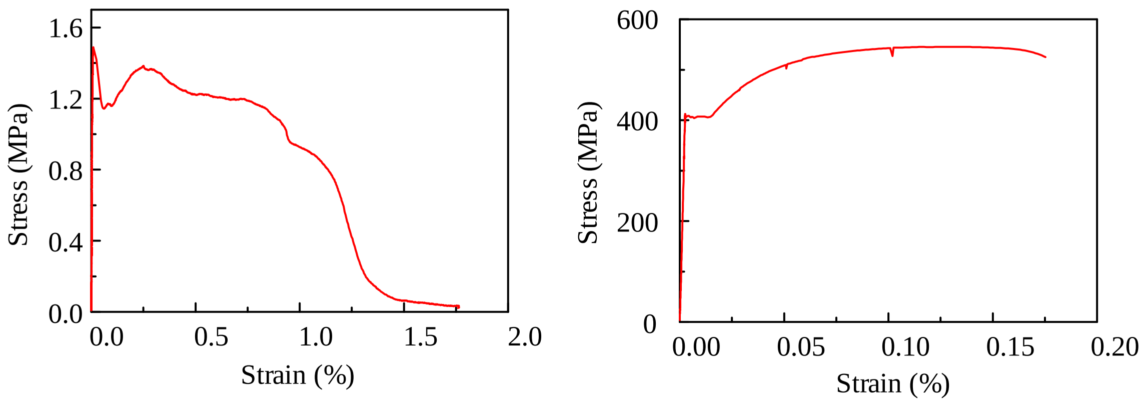

(a) ECC (b) Steel

Fig. 3. Typical tensile stress–strain curves of materials in the test.

2.3 Test procedure, set-up and instrumentation

Vertical uniform loads and lateral cyclic loads were applied successively in the test, whose structural behavior under the slab loads and seismic loads were investigated, the loading history is plotted in Fig. 4. Specifically, uniform loads were imposed by iron blocks during the vertical loading cases, the loading slab was located at the length of 1950 mm of the middle longer span. The final vertical weight on the slab was 5.82 t due to the limitation of loading space and consideration of test safety. After the vertical loading, 0.5 t uniform load was retained, which was kept in the following loading step to simulate the common design load in engineering referring to GB 50009-2012 [30]. Then, axial forces transferred from the superstructure were simulated in the test to reflect the actual mechanical state of the columns in the real structure. Column compression forces were applied to the side and middle column, which were 150 kN and 300 kN, respectively (the axial compression ratio was 0.1, and 0.2 for the latter). Fig. 4 plots the cyclic loading protocol, which followed the force-displacement mixed control loading method [31].

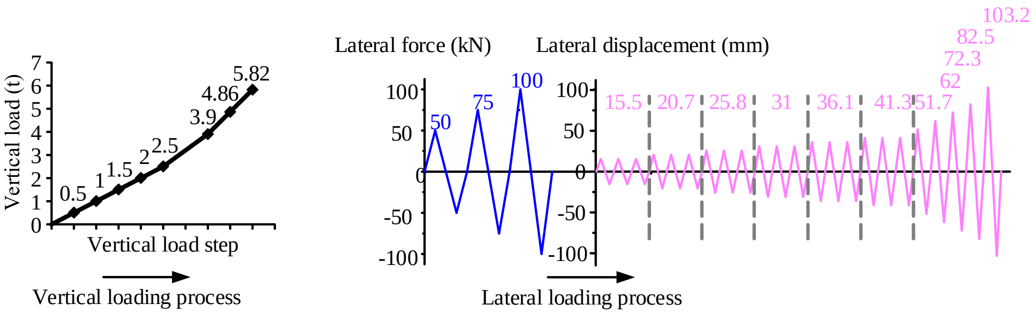

Fig. 4. Vertical and lateral loading history.

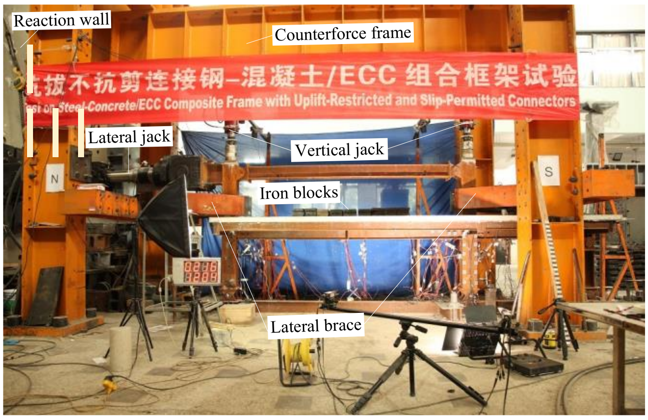

Fig. 5. Test set-up.

The test set-up is depicted in Fig. 5. The test was loaded by iron blocks, as well as the vertical and lateral jacks, which were connected with the counterforce frame and reaction wall, respectively. Two lateral braces were applied to avoid out-of-plane deformation of the specimen.

Fig. 6 illustrates the measuring arrangement of the specimen. Displacement meters, strain gauges were instrumented to obtain test data mainly including the displacement, deflection, and strain. The displacement meter, which was connected with two guide bars attached to the concrete and steel beam respectively, was used to acquire the interface slip of composite beam. The inclinometers near the beam-column joints were installed to acquire the relative rotation data of the joints for future research. The cracks on the slab were observed and recorded by crack measuring devices after each loading level.

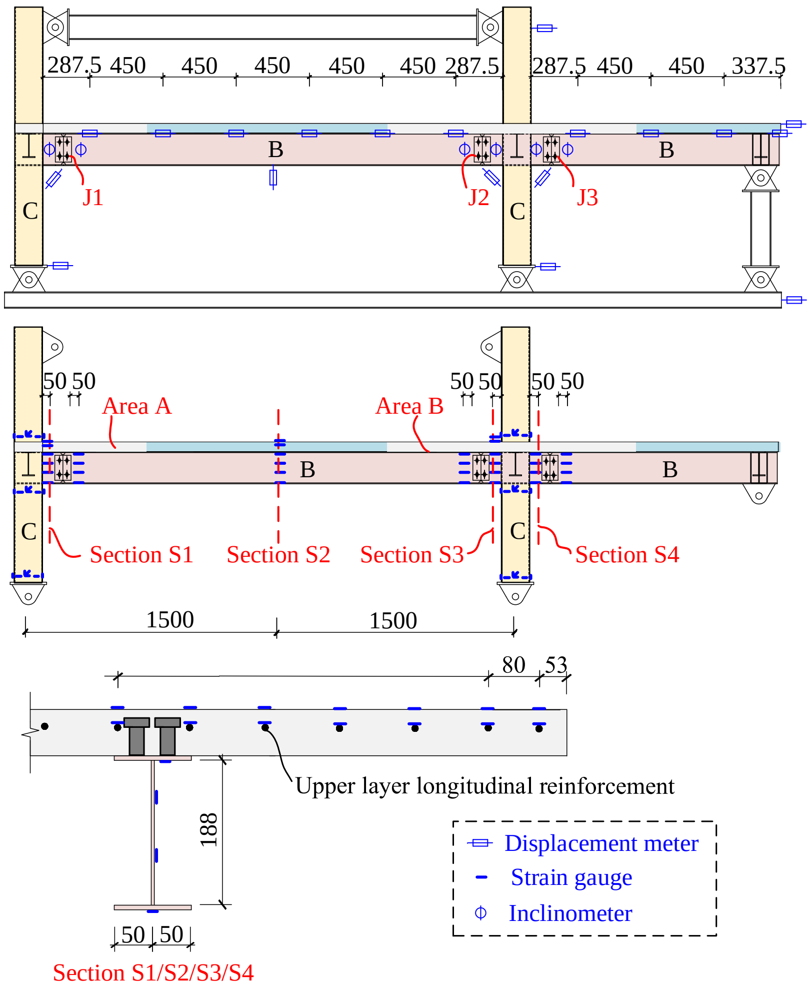

Fig. 6. Arrangement of measuring equipment (in units of mm).

3. Test results and discussion

3.1 Failure modes of Specimen SCUE

The test results of Specimen SCUE with ECC and URSP-S connectors near the column are reported below. In the first cycle corresponding to a displacement level of 15.5 mm (abbreviated as 15.5(1), similar abbreviations hereafter), an obvious sound could be heard. In the positive loading of 25.8(1), the capacity has a drop point, and a large area of weld cracking appeared at the bottom flange steel plate of the joint J1 (J1, is marked in Fig. 6, as well as J2 and J3 hereafter) near the side column. In 25.8(2), accompanied by banging noise, the weld at the bottom flange steel plate of J1 was completely ruptured, which is depicted in Fig. 7(a). Similar welds ruptures could be observed at two bottom flange steel plates of joints J2 and J3 near the middle column. The weld of J2 has partially pulled apart in negative loading of 31(1) and completely fractured in negative loading of 31(3), which is shown in Fig. 7(b). In the negative loading of 36.1, the bottom flange steel plate of J3 buckled and a complete weld fracture happened in 41.3(2), which is depicted in Fig. 7(c). In the positive loading of 72.3, substantial cracks including longitudinal cracks were found on the slab near the north of the middle column. In the negative loading, substantial cracks including longitudinal cracks were observed on the slab near the side column, and new cracks occurred on the slab near the south of the middle column. After the test loading, as Fig. 7(d) and (e) show, slight crush and cracking phenomena were observed on the slab near the columns, demonstrating that the slab damage was controlled well with ECC and URSP-S connectors.

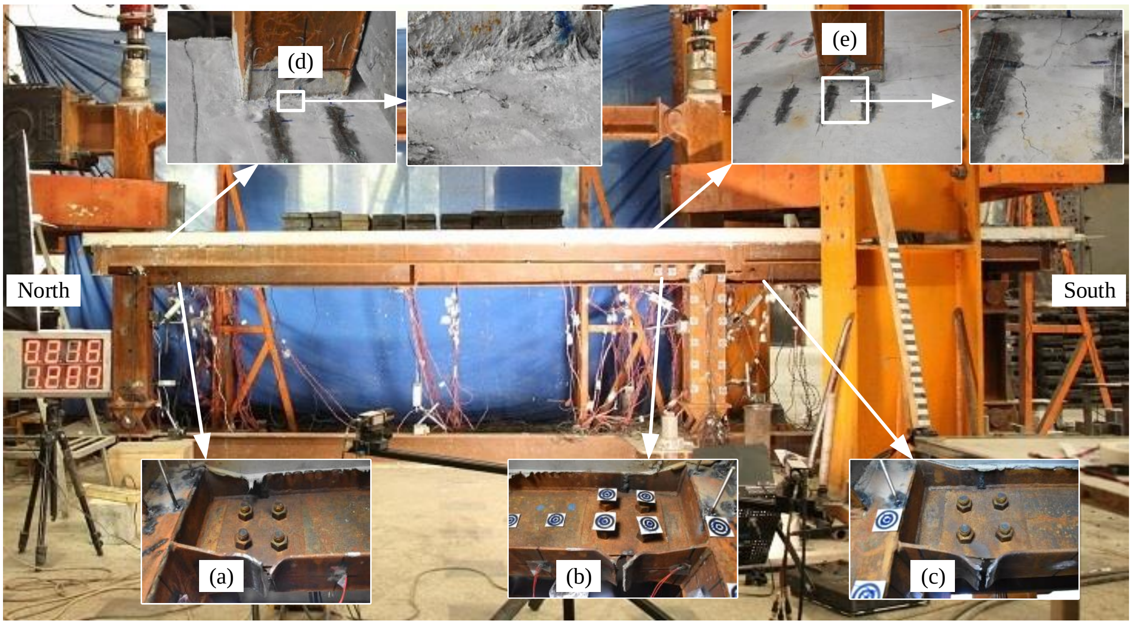

Fig. 7. Failure phenomenon of Specimen SCUE after the test.

Before loading, only one initial crack was observed on the slab (as shown in Fig. 8(a)) owing to the use of ECC and URSP-S connectors. Several cracks gradually appeared on the slab during vertical loading cases. When vertical load was 5.82 t, the crack patterns were plotted in Fig. 8(b). At the displacement of 25.8 mm, several transverse and oblique slab cracks were found near the columns, while still few longitudinal cracks were emerged (as shown in Fig. 8(c)).

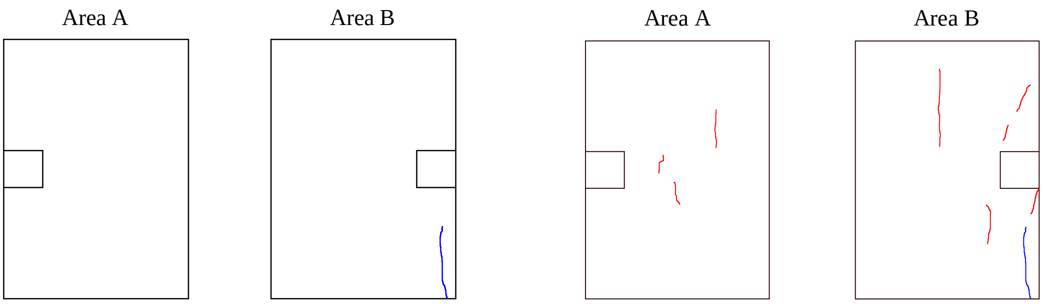

(a) Before loading (b) Vertical loading (5.82 t)

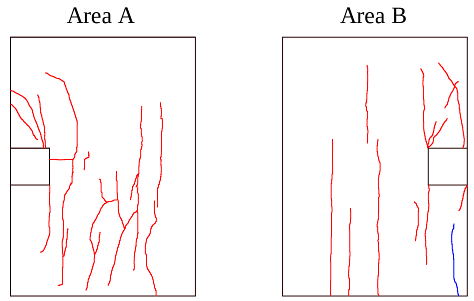

(c) Lateral loading (25.8 mm)

Initial crack New crack

Fig. 8. Crack patterns of Specimen SCUE.

3.2 Hysteretic behavior of Specimen SCUE

The hysteresis and skeleton curve are depicted in Fig. 9. The skeleton curve is obtained through the connection of the peak load point of each displacement loading of the hysteresis curve. Welding fractures at beam-to-column connections caused a sharp decrease in the load capacity of the specimen. As the loading progressed, the force state of the specimen was gradually from elastic-plastic to the plastic stage since the slab had already cracked in the vertical loading cases.

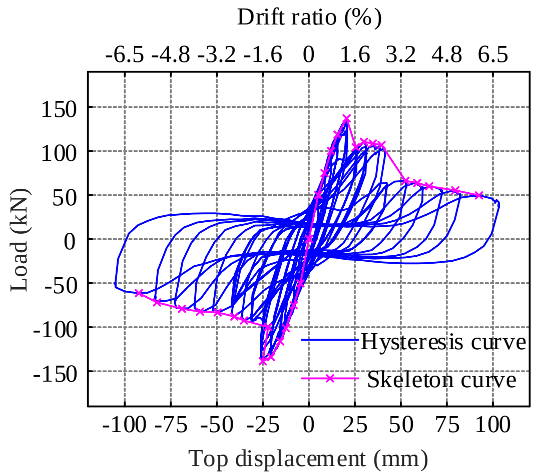

Fig. 9. Load-displacement curves of Specimen SCUE.

At a certain loading grade, the strength of the structure decreases with the number of loading cycles increasing. The strength degradation coefficient η (for a certain loading grade, the strength of the second/third cycle divided by the first cycle) is used to evaluate the strength degradation. Fig. 10(a) plots the strength degradation coefficient of Specimen SCUE under positive and negative loads. The results show sustained strength degradation, and a plunge was observed when the fracture occurred at the steel plate of joints.

Under lateral cyclic loads, as the loading process increased, the stiffness of the structure decreased. The looped stiffness k_l (for a certain loading grade, the sum of peak loads of three cycles divided by the sum of displacements) is used to evaluate the stiffness degradation. Fig. 10(b) gives the looped stiffness of each drift ratio of the Specimen SCUE. The results indicate evident and steady stiffness degradation throughout the whole test.

The energy dissipation is defined as the area surrounded by the hysteresis loop and the horizontal axis [16]. E_h, E_c denotes the energy dissipation of the loading half-cycles n_h and the accumulation from starting point of loading to n_h, respectively. As the loading half-cycles n_h increases, the development of E_h and E_c of the Specimen SCUE, as illustrated in Fig. 10(c). The results show that the accumulation energy dissipation E_c increased steadily throughout the whole load period, while the energy dissipation of the loading half-cycle E_h decreased in the later loading stages, which was affected by the capacity of the specimen.

Viscous damping coefficient h_e, whose definition can refer to [16], is adopted to access the energy dissipation. Fig. 10(d) plots the development curve of h_e with the increase of the loading cycles n of the Specimen SCUE. The results show that h_e was between 0.1-0.3 and decreased at the time of the steel plate fracture of joints in the test.

Generally, the stable strength, stiffness degradation and energy dissipation show that the new structure with ECC and URSP-S used near the column has a good seismic performance.

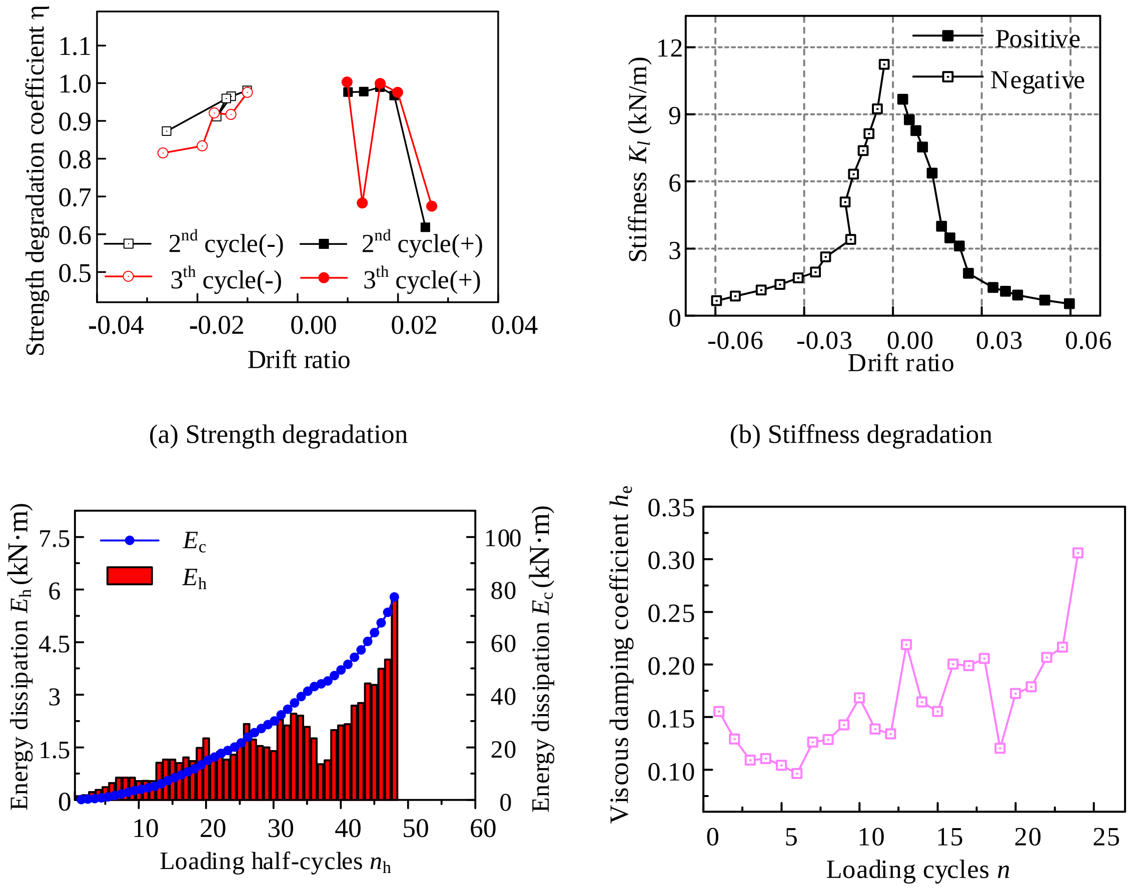

(a) Strength degradation

(b) Stiffness degradation

(c) Dissipated energy

(d) Viscous damping coefficient

Fig. 10. Stiffness, strength degradation and dissipated energy of Specimen SCUE.

3.3 Steel strain of Specimen SCUE

Under the vertical load cases, the strains of steel beam of key sections S1, S2 and S3 are gauged, as illustrated in Fig. 11. The location of the three key sections is marked in Fig. 5. The results of Fig. 11 indicate that the strains of the three sections of the steel beam were basically conformed with the plane section assumption. Moreover, the maximum steel strain under the vertical load condition was much smaller than the yield strain (1743 με, 1951 με for web and flange plate of steel beam, respectively). The strain of the steel beam was consistent with the structural force analysis result in terms that sections S1 and S3 bear negative bending moment while section S2 was under a positive moment. The results of Fig.

11 (c) show that all the steel strain of section S2 was tensile under the vertical stacking load. This indicates that the neutral axis was located in the slab, which conformed to the theoretical analysis of the composite beam. From Fig. 11(a) and (b), it is found that the negative bending moment of section S1 was smaller than that of section S3 when subjected to vertical uniform loads, which was consistent with the force analysis of the frame beam with asymmetric boundary (see Ref. [21]).

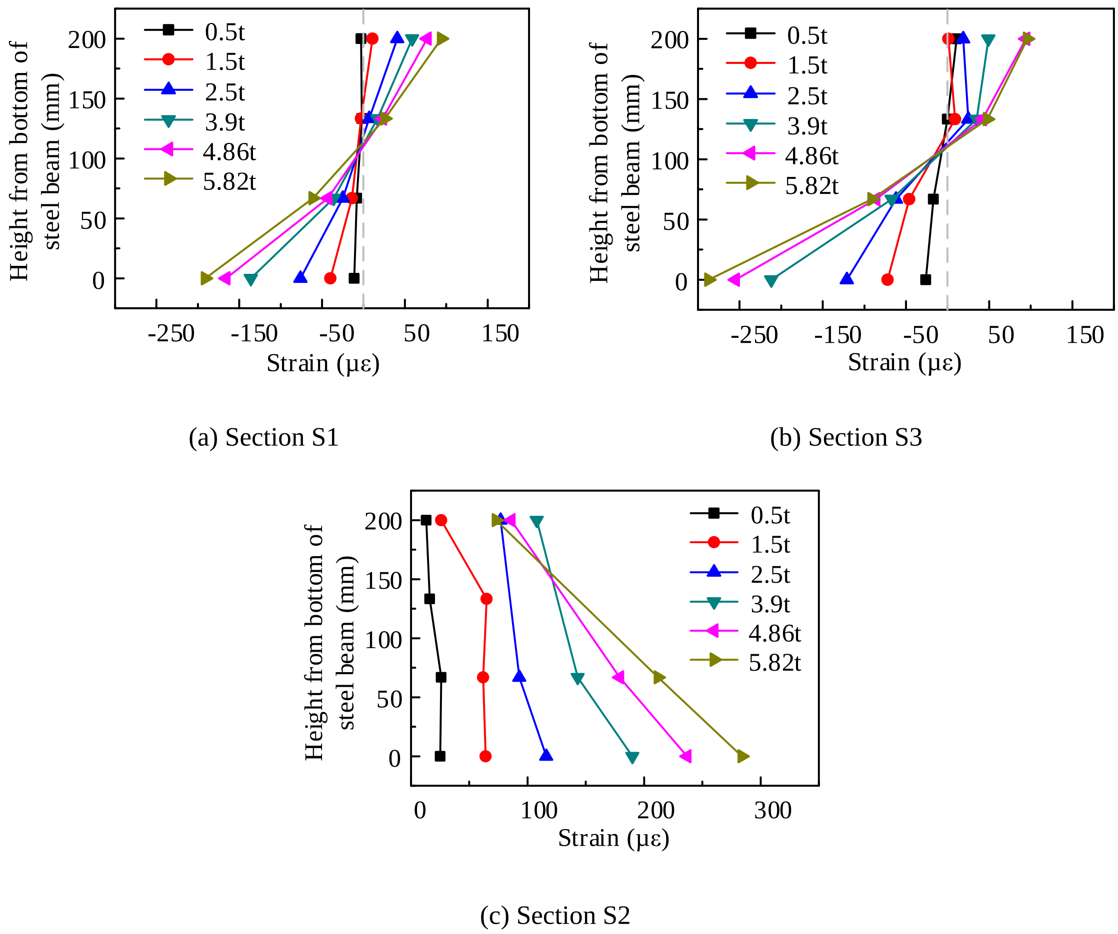

Fig. 11. Steel beam strain of three key sections of Specimen SCUE.

During the cyclic lateral loading, the strain of the steel beam bottom flange bore tension and compression cyclically in positive and negative directions, the strains of Sections S1, S3 and S4 are illustrated in Fig. 12. The loading displacement level corresponding to weld fracture of three joints J1, J2 and J3 are also marked in this figure. The results show that the compressive strain had already exceeded yield before the weld fracture, which indicates that the poor weld quality did not affect the hogging moment capacity at the three sections. After the weld fell apart, the tensile and compressive strains were both sharply decreased.

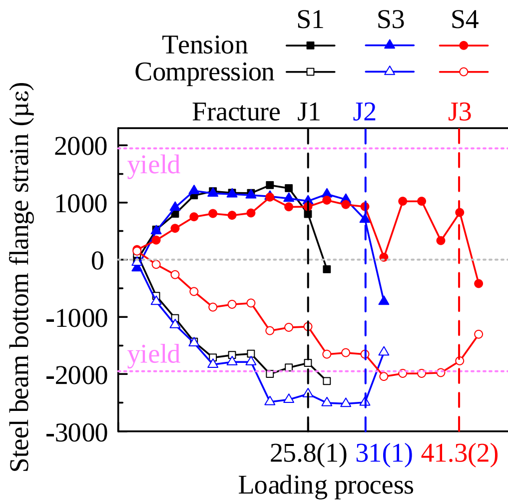

Fig. 12. Strain development of steel beam bottom flange of Specimen SCUE.

When subjected to negative loading, Sections S1 and S4 were under hogging moment and the rebar strains were tensile. The rebar tensile strain distribution along transverse direction is plotted in Fig. 13. As the distance from the centerline of the beam increased from 150 to 550 mm, the rebar strain gradually decreased, demonstrating an obvious shear lag effect of the ECC slab. It should be mentioned that lower strains were observed at a distance of 50 mm in most loading cases possibly because of the fracture of the welding spot connecting the reinforcement and column.

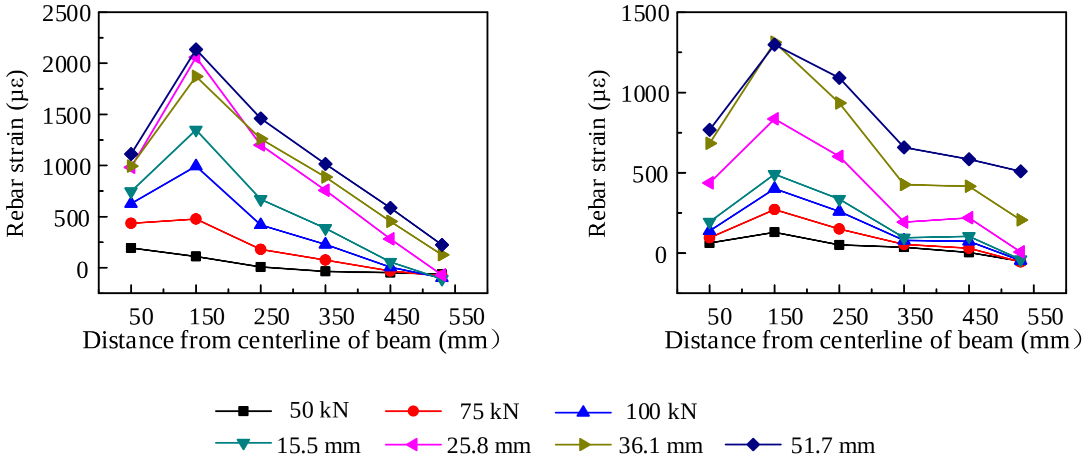

(a) Section S1 (b) Section S4

Fig. 13. Rebar strain distribution along transverse direction of Specimen SCUE.

3.4. Comparison of five specimens

3.4.1 Load-displacement hysteretic behavior

To investigate the influence of ECC and URSP-S connectors on the performance of frames, test results of five specimens were compared and analyzed. Fig. 14 illustrates the skeleton curves of five specimens. Table 5 gives several important indexes based on the skeleton curves. The yield load and displacement could be obtained by the graphical method [19, 32]. The ultimate capacities of specimens with ECC or URSP-S connectors were compared quantitatively with Specimen SC in Table 5. It turns out that the ultimate capacity of Specimen SCUE with ECC and URSP-S connectors was close to Specimen SC with concrete and conventional studs, where the difference was within 10%. Similar findings were observed for specimens with ECC or URSP-S connector only.

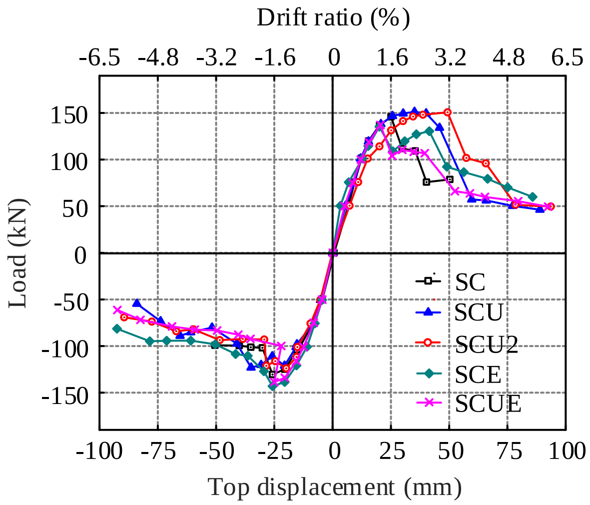

Fig. 14. Skeleton curves of five specimens.

Table 5 Summary of test results of five specimens.

Specimen		Yield load P_y (kN)	Ultimate load P_u (kN)	$\frac{P_u}{P_{u,SC}}$	Yield displacement Δ_y (mm)	Ultimate displacement Δ_u (mm)	85% of ultimate displacement Δ_d (drift ratio)	$\frac{\Delta_d}{\Delta_y}$
SC	Positive	129.9	145.8	1	18.2	25.1	28.2(1.8%)	1.55
	Negative	115.4	130.1	1	18.1	25.8	28.8(1.9%)	1.59
SCU	Positive	131.2	151.2	1.04	18.7	35.1	46.9(3%)	2.51
	Negative	114.0	123.2	0.95	18.8	35.0	39.4(2.5%)	2.10
SCU2	Positive	135.0	150.8	1.03	26.2	49.3	53.0(3.4%)	2.02
	Negative	118.1	124.0	0.95	17.8	19.9	28.9(1.9%)	1.62
SCE	Positive	116.7	135.4	0.93	15.8	20.0	44.5(2.9%)	2.82
	Negative	129.6	143.1	1.10	18.0	25.8	31.7(2%)	1.76
SCUE	Positive	122.9	137.1	0.94	16.7	20.5	23.6(1.5%)	1.41
	Negative	133.5	138.7	1.07	20.4	25.0	23.4(1.5%)	1.15

3.4.2 Cracks width and numbers

Under vertical loads, the crack width and number on the slab of five specimens are shown in Fig. 15(a) and (b), respectively. (i) Crack width (see Fig. 15(a)). Compared with Specimen SC, the crack width of the other four specimens was less, indicating that ECC and URSP-S effectively decreased the crack width. Comparing Specimens SCU and SCE, it is found that ECC had a better control effect than URSP-S when applying the same half-span length. Among five specimens, the result of Specimen SCUE was the lowest, indicating that using half-span ECC and URSP-S connectors simultaneously significantly diminished the crack width. Specifically, when the load was 5.82 t, corresponding crack width of Specimen SC, SCU, SCU2, SCE and SCUE were 0.22, 0.2, 0.2, 0.18 and 0.1 mm, respectively. The decrease in crack width of Specimen SCUE after using ECC and URSP-S connectors was 55% in comparison with Specimen SC. (ii) Number of cracks (see Fig. 15(b)). The largest number of cracks were found in Specimen SCE, indicating the application of ECC increases the number of new cracks, which was also stated in Ref. [16]. The number of cracks of Specimen SCUE was much less than Specimen SCE, indicating the number of new cracks of the specimen with ECC was significantly reduced because of the use of URSP-S connectors, which also means the number of cracks was well controlled when ECC and URSP-S connectors were both used at the same time.

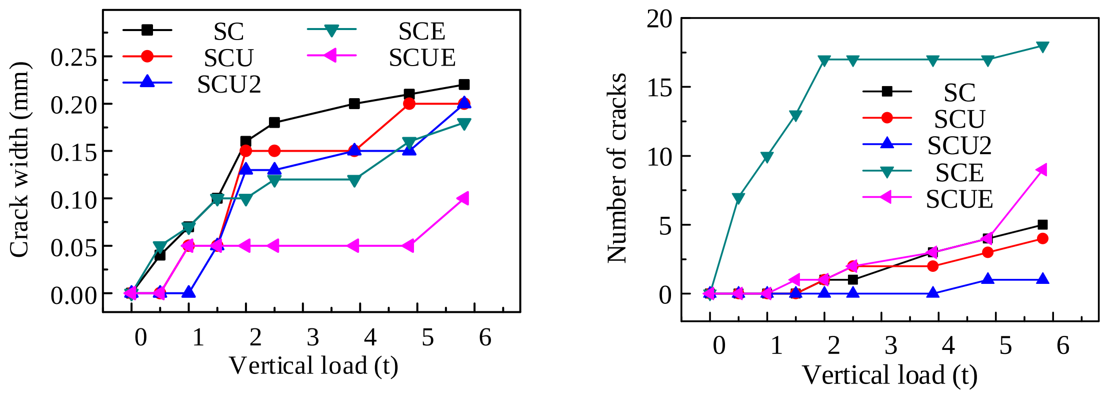

(a) Crack width (b) Number of cracks

Fig. 15. Crack comparison under vertical loading cases.

With the increase of the lateral displacement, the development of the crack width on the slab is plotted in Fig. 16. The result of Specimen SCUE was minimal, indicating the crack width can be well controlled using both ECC and URSP-S. The width of cracks of Specimen SCE was less than SCU, indicating that ECC reduced the crack width more significantly than URSP-S with the same application length. It can also be observed that little difference was found between results of Specimen SCE and SCUE, which means that after half-span ECC was used, half-span URSP-S had little effect on improving crack width control.

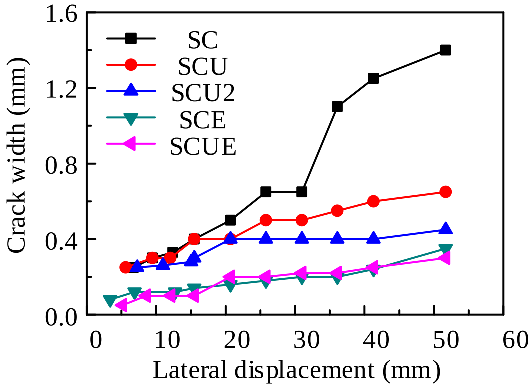

Fig. 16. Crack comparison under lateral loading cases.

The results in terms of the crack control effects under the whole loading process show that ECC played a major role in width of crack while URSP-S connectors played a major role in number of crack. Anyhow, the development of crack widths and numbers were well controlled at the ultimate state and the end of loading when both the half-span ECC and URSP-S were arranged in composite frames.

3.4.3 Interface slips

Under vertical loads, the maximum interface slip of the composite beam of five specimens are compared: SC(0.634 mm), SCU(0.844 mm), SCU2(1.57 mm), SCE(1.217 mm), SCUE(3.728 mm). From the previous studies [16, 21], it has been found that the URSP-S connectors and ECC increased the interface slip compared with the basic Specimen SC. Here, comparing Specimen SCE with ECC and Specimen SCU with URSP-S connectors, it is found that the increase of slip applying ECC was higher than that applying URSP-S connectors. For Specimen SCUE with ECC and URSP-S, the slip increased significantly due to the superposition effect of ECC and URSP-S. Similar regularity can be found for lateral loading cases. The corresponding slip of the five specimens at the ultimate bearing capacity are SC(0.89 mm), SCU(1.04 mm), SCU2(2.73 mm), SCE(1.281 mm), SCUE(4.662 mm). It should be mentioned the large slip of frame using ECC and URSP-S connectors rarely influenced the failure mode and integrity of structural behavior during the whole loading test.

4. Finite element

4.1 Finite element modelling and validation

The elaborate finite element (FE) model of the specimen was developed using nonlinear finite element software, MSC.Marc [24], and simulating models were supplementary analyzed to explore the capacity of steel-concrete frames with ECC and URSP-S under various parameters.

4.1.1 Loading and boundary conditions

The assembled FE model was properly restrained, which was consistent with that in the experiment, as illustrated in Fig. 17. The bottom of the column was constrained by constraints UX=UZ=0 on the central y-axis. UZ=0 at beam end was set. UY=0 on the column was simulated to the transverse constraint. The vertical load was exerted on the slab, axial load was imposed on the column, and lateral displacement was applied to the side column.

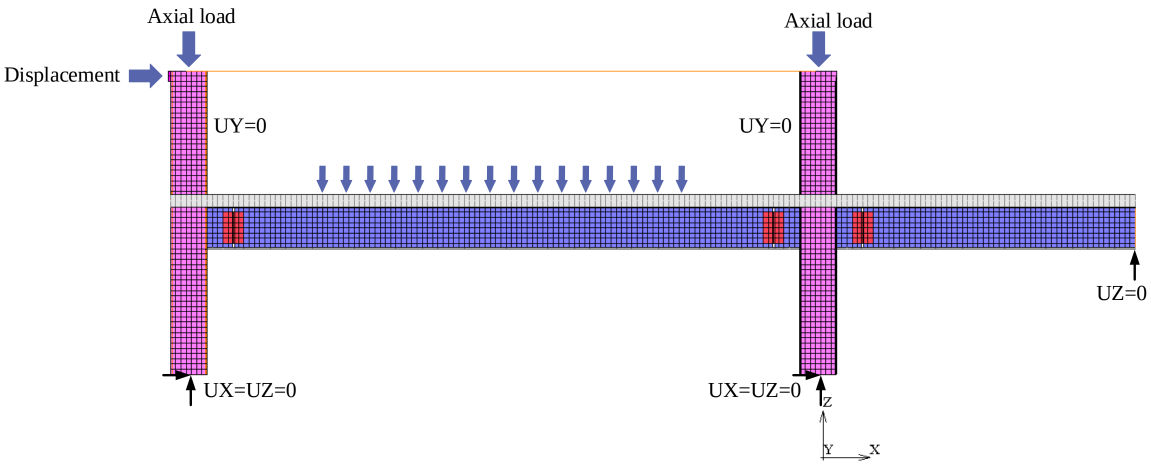

Fig. 17. Boundary conditions in FE models.

4.1.2 Finite element type

The three-dimensional refined modeling can reflect global and local effect between components of steel-concrete composite structure accurately [33, 34]. However, considering higher computing efficiency, shell elements were mainly applied in this modeling and has been used in previous studies [3, 35]. In detail, shell elements were used for the steel tube of CFST columns and steel beams, solid elements were adopted for the core concrete of CFST columns. For CFST columns, the core concrete shared nodes with steel tube, the modelling strategy rarely influences the frame behaviour [4]. The use of layered shell elements has been proven to simulate the spatial combination effect of floor slabs accurately and improve computing efficiency [4]. No. 75 layered four-node thick-shell elements with six degrees of freedom per node using full integration schemes were employed for the concrete/ECC slab along the thickness direction as per Ref. [4]. The corresponding proportions of concrete/ECC, longitudinal and transverse rebar material layers of the layered shell element were calculated based on Ref. [36] (see Fig. 18 (a)). The element mesh size was generally 25 mm. A x-axis truss element, connecting nodes on the central y-axis, was applied to simulate the horizontal rod connected the columns. The shear connectors inside the composite beam were simulated by the longitudinal and vertical springs (see Fig. 18 (b)).

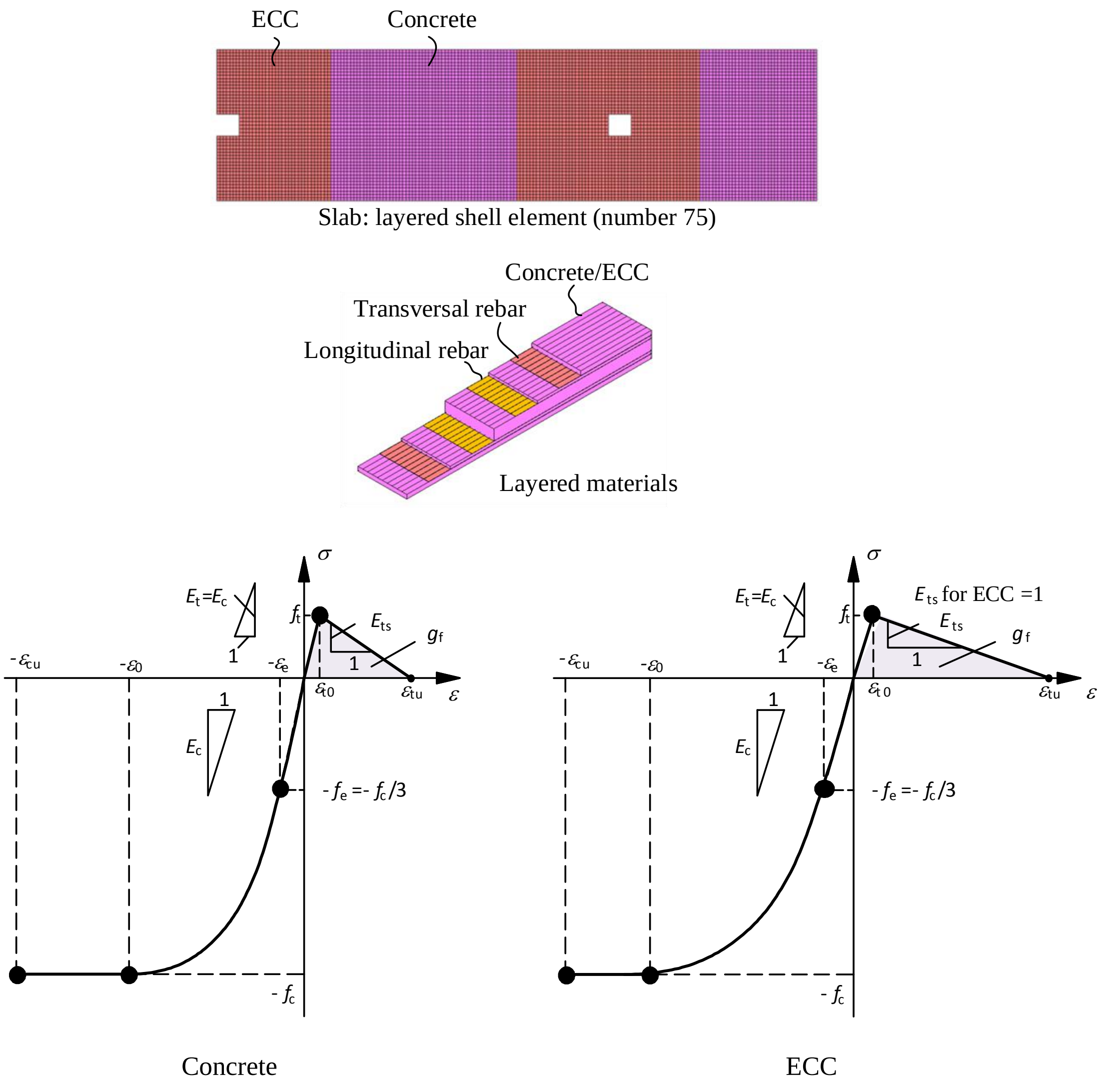

(a) Slab modeling and the stress-strain curve of Concrete/ECC

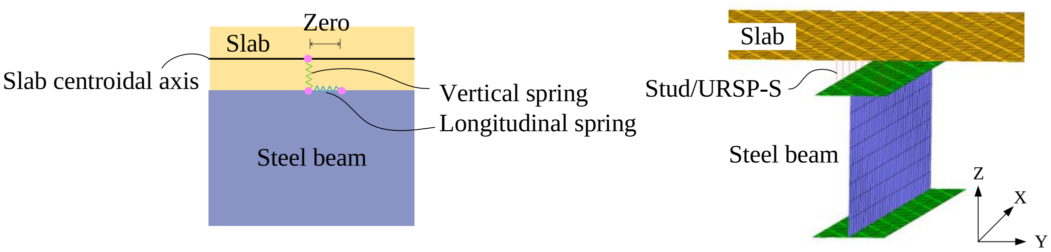

(b) Shear connectors modeling

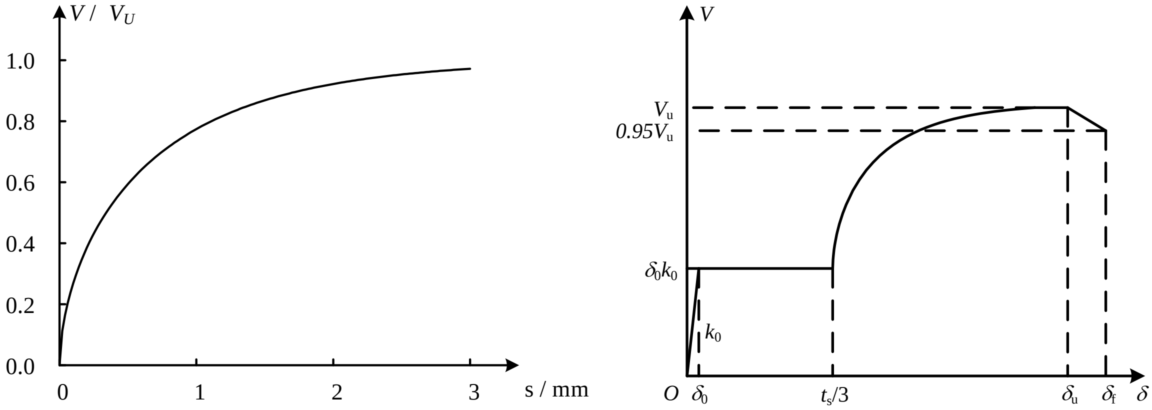

(c) Constitutive curve of shear stud (d) Constitutive curve of URSP-S connector

Fig. 18. Modeling details in the FE models.

4.1.3 Material modeling

The elastic material was adopted in the simulating of column concrete on the basis of design criterion of "strong-column-weak-beam" and the test results that no yield was found in the CFST column. Rüsch curve was employed as the constitutive relationship of the slab concrete [37], see Fig. 18(a). For ECC, the stress-strain curve form similar to that of concrete and different value of key parameters of the curve was adopted. The material properties were the same as the ECC material test results. The elastic modulus E_s took a value of 20 GPa recommended by Ref. [8, 38], and the tensile softening modulus E_{ts} was set as 1 MPa when simulating ECC under tension [16]. The three-fold line constitutive law was used for the steel plate [4], the constitutive law of reinforcement in tension and compression in Ref. [16, 39] was adopted. The material properties were the same as those in the test. The steel plate fracture of beam flange was not considered in FE modeling and did not influence the research aim in this paper. Fig. 18(b) gives the simulation of shear connectors in composite beam. The constitutive curves proposed by Ollgaard et al. [40] and described in Ref. [19] were employed for shear studs and URSP-S connectors, respectively in the simulation, as depicted in Fig. 18(c) and (d).

4.1.4 Validation of FE model

Fig. 19 shows the experimental and numerical comparison of the hysteresis curves of Specimen SCUE in lateral loading cases. It is found that the initial stiffness and the capacity were in good agreement with the test results, indicating the responses were accurately simulated by using the established models. It should be mentioned that the data of larger loading displacement in FE was missing because of the unstable convergence of the FE modeling. This rarely affects the research aim focusing structural capacity. In addition, the stiffness degradation curves of Specimen SCUE by test and FE were compared, which showed good consistency as shown in Fig. 20. The validation of other specimens can be shown in previous study by the authors [16].

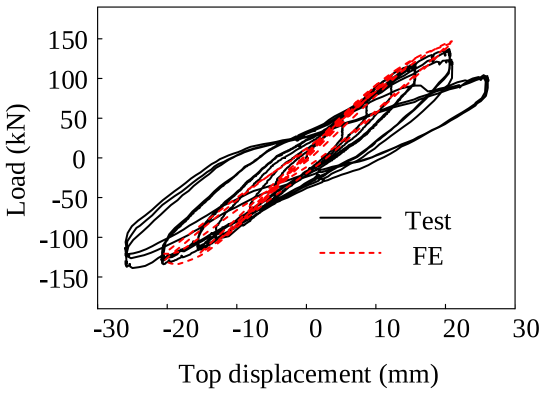

Fig. 19. The load-displacement curves of Specimen SCUE by test and FE.

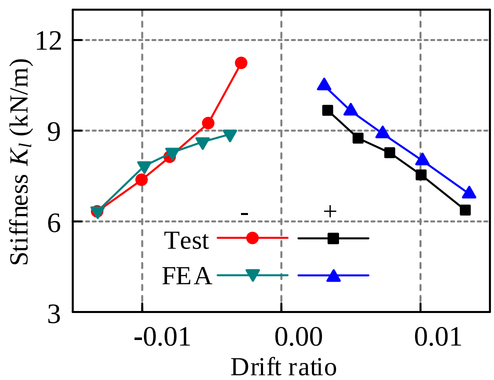

Fig. 20. The stiffness degradation curves of Specimen SCUE by test and FE.

According to the FE results, the bending moment diagrams of the frame at the loading displacement of peaking loads in positive and negative directions are plotted in Fig. 21(a) and (b), respectively. The bending moments of each component truly reflected the structural force of experimental specimen. When the frame reached ultimate capacity, the sagging moment of composite beam end near the side and middle columns were 78 and 48 kN·m, respectively. The larger sagging moment of the beam end occurred near the side column in the positive loading, which was in line with the test results that welding fracture firstly happened at the joint near the side column. At the peak point of the skeleton curves, the stress near the side column in positive loading and the middle column in negative loading in FE results are given in Fig. 22(a) and (b), respectively. It is found that the column kept elastic and the lower flange of the steel plate where the welding fracture of the joint occurred in the test exceeded yield. FE results of equivalent Von Mises stress of slab upper layer reinforcement at the positive and negative ultimate capacity are given in Fig. 22(c). Large slab stress occurred near the columns, where the failure of the slab occurred in the test. Furthermore, the local slab-interaction effects of steel-concrete composite joints and the resisting mechanisms were studied comprehensively in Ref. [41]. In all, the above-mentioned FE results show that the overall behavior and damage concentration of the specimen were well reproduced, demonstrating the accuracy of the established FE model. It should also be mentioned that a sudden stress increase was found at the interface of the arrangement of ECC/URSP-S and concrete/studs, indicating the complex stress of the interface and needed to be further studied. However, no obvious phenomenon was found at the interface in the test.

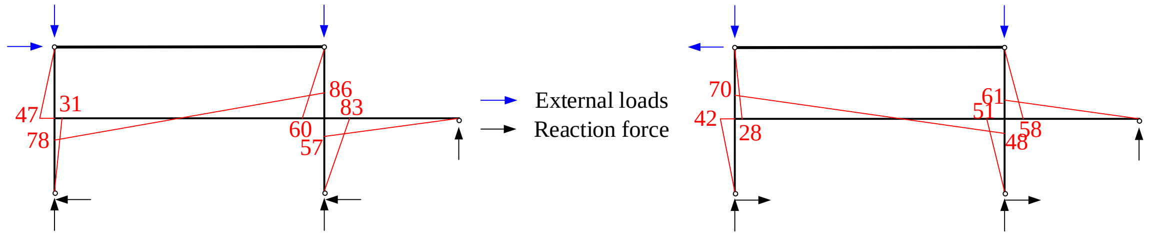

(a) Positive loading (b) Negative loading

Fig. 21. Bending moment diagram of Specimen SCUE at the ultimate capacity (in units of kN·m).

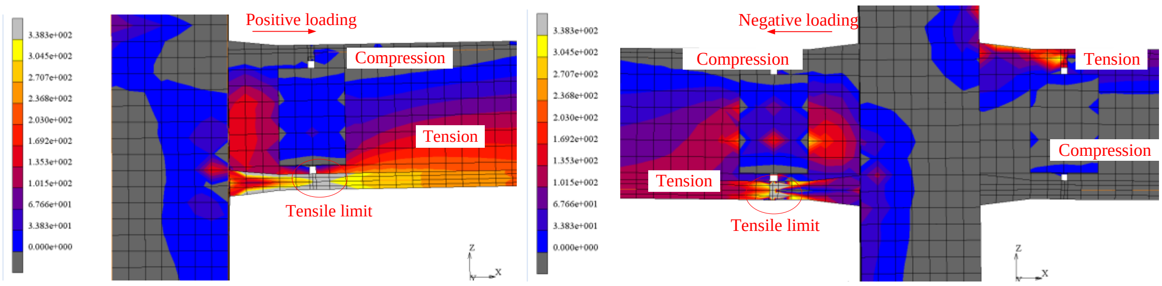

(a) Stress near the side column (b) Stress near the middle column

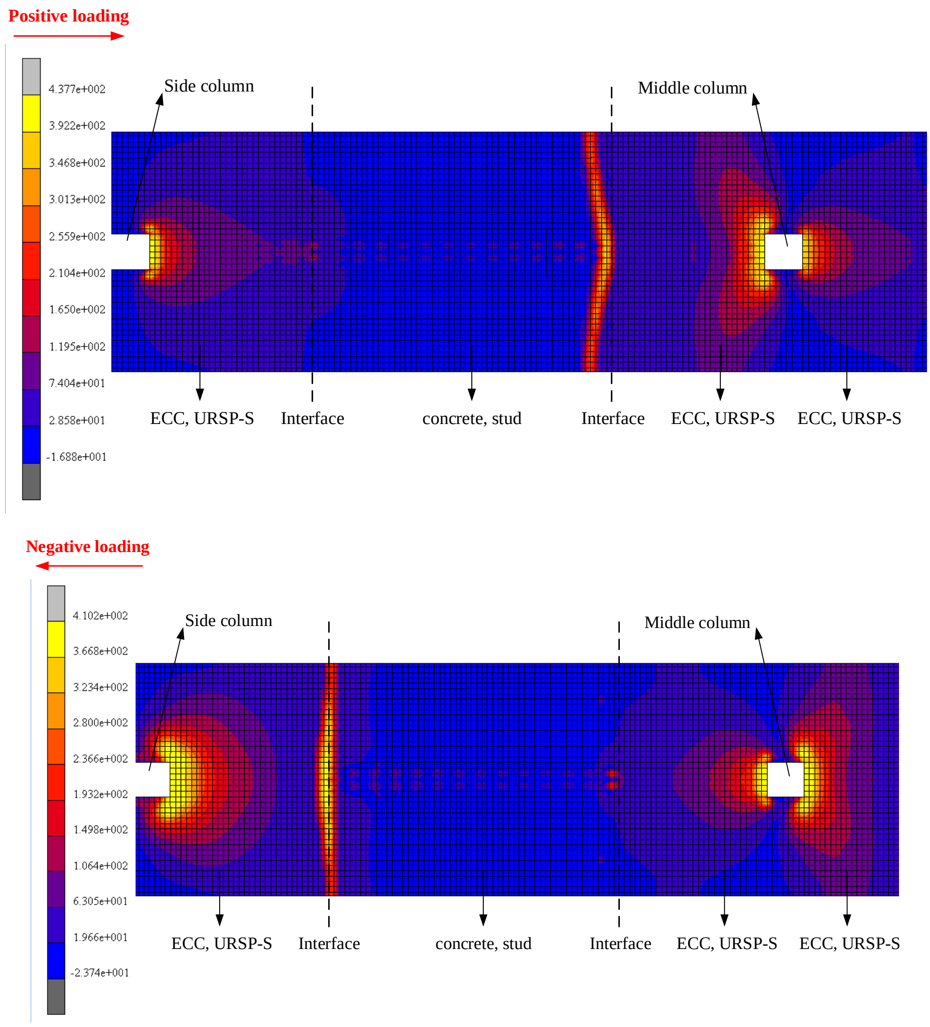

(c) Equivalent Von Mises stress of slab upper layer reinforcement of positive and negative loading

Fig. 22. FE results of Specimen SCUE at the ultimate capacity.

4.2 Capacity of the specimen frame under various parameters

To explore the influence factor of the capacity of steel-concrete-ECC composite frames with URSP-S connectors, parametric analysis was performed emplying the validated FE model. The parameters included ECC properties (tensile and compressive strength), slab dimensions (thickness and width), shear connector degree, longitudinal reinforcement ratio and steel beam (yield strength of steel beam flange and height). As listed in Table 6, the initial values of parameters were determined in according with test specimen, and these ranges of the parameters covered most of the common engineering practice values. The column was assumed to be elastic during the simulation, which was consistent with the actual test. Therefore, the parameters related to the column were not considered in the analyses.

Table 6 Parameters considered in the supplementary models.

Parameters	Values (Bold font represents the initial values)
ECC tensile strength (MPa)	2, 3, **4**, 5
ECC compressive strength (MPa)	35, **55**, 75, 95
Slab thickness (mm)	40, 50, **60**, 70
Slab width (mm)	900, **1100**, 1300, 1500
Shear connector degree	Partial, **full**
Longitudinal reinforcement ratio	1.7%, **0.94%**, 0.6%
Steel yield strength of steel beam (MPa)	300, 350, **400**, 450
Steel beam height (mm)	150, **200**, 300

To quantitatively evaluate the influence factor of the frame capacity, the relative difference between the results of each case and the initial value is calculated and given in Fig. 23(a) and (b). The relative difference d_{i} of a certain case is defined as

$$d_{\mathrm{i}} = \frac{F_{\mathrm{i}} - F_0}{F_0} \tag{1}$$

Where F_i, F_0 are the frame capacity result of a certain case and the result using the initial value by simulation, respectively, and parameters of simulating cases are shown in Table 6.

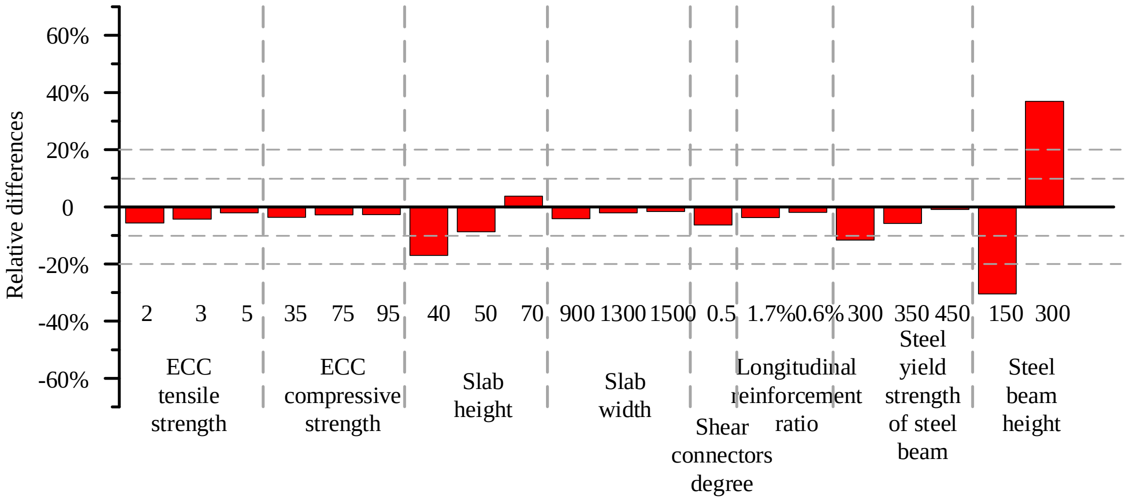

(a) Capacity differences in the positive loading direction

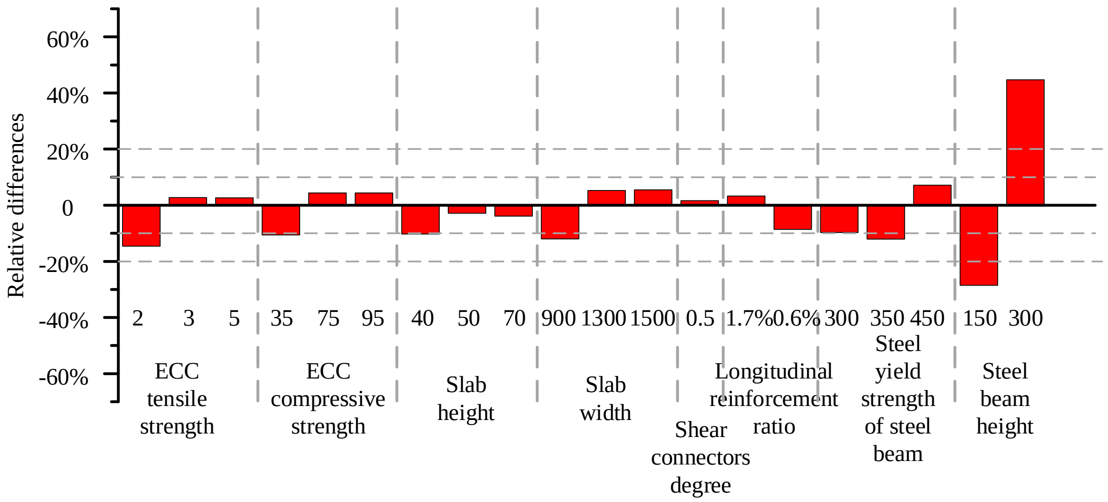

(b) Capacity differences in the negative loading direction

Fig. 23. Influence factors of the capacity of the frame.

In the positive loading, the slab height, steel yield strength and steel beam height influenced the structural capacity, whose relative differences were greater than 10% within their variation range, while the other factors did little influence on the frame capacity. In the negative loading, many factors influence the capacity including ECC tensile strength, slab width, steel yield strength and height of steel beam. The relative differences of these parameters within their variation range were between 10%-20% except for the steel beam height. Generally, the frame capacities in the positive and negative direction were mainly affected by the steel beam height. The influence of these factors on the capacity of the frame was through their influences on the beam. Since the effect of the properties of the slab on the beam subjected to hogging moments was larger than sagging moments, and the structural bending moment diagrams plotted in Fig. 21 show that there were two hogging moments in the negative direction while one hogging moment in the positive direction. Therefore, the capacity in the negative direction was more affected by the material properties of the slab.

5. Conclusion

In this study, a steel-concrete-ECC composite frame with URSP-S connectors was proposed and was experimentally studied with a large scale of 1/2 under vertical uniform loads and lateral cyclic loads. The experimental results were analyzed and also compared with those of different slab materials and shear connectors. Moreover, FE models of the specimen frame were established and parametric analysis in terms of the capacity of the frame was performed. Main conclusions can be drawn as follows:

1. The novel frame with ECC and URSP-S connectors behaved well and had good seismic performance in terms of hysteretic behavior, stiffness, strength degradation and dissipated energy. Plane section assumption was met at the early loading stage and the shear-lag effect was found in the slab of this novel frame.
2. The comparison of the results of five specimens with different slab material and shear connectors show that ECC and URSP-S connectors enhanced substantially the crack

resistance of slab while influencing the capacity of the frame within 10%. Specifically, the decrease in crack width of the slab after using half-span URSP-S connectors and ECC simultaneously in the frame was 55% when subjected to 5.82 t vertical load in the test. The increase of crack number due to use of ECC was controlled well after applying URSP-S connectors. ECC played a major role in controlling the crack width while URSP-S connector played a major role in controlling the crack number. Furthermore, URSP-S connectors and ECC increased the interface slip without influencing the structural failure modes.

3. The established elaborate FE models can simulate the overall behavior and damage concentration of the frame specimen effectively. The parametric analysis results by FE show the capacity of the novel frame was mainly affected by the steel beam height.

On the basis of the limited number of test specimens, the results show that the steel-concrete-ECC composite frame with URSP-S connectors has good performance, and ECC and URSP-S connectors enhanced the crack resistance effectively. In the future, the specific and reasonable arrangement of ECC and URSP-S connectors of the entire composite structure to provide guidance for engineering design is need to be explored.

Acknowledgments

This research was supported by the National Natural Science Foundation of China (Grant Nos. 51978377 and 52108153). The financial support is gratefully acknowledged.

References

[1] Elghazouli AY, Castro JM, Izzuddin BA. Seismic performance of composite moment-resisting frames, Eng Struct 2008;30(7):1802-19.

[2] Spacone E, El-Tawil S. Nonlinear analysis of steel-concrete composite structures: State of the art. J Struct Eng 2004;130(2):159-68.

[3] Nie JG, Huang Y, Yi WJ, Fan JS. Seismic behavior of CFRSTC composite frames considering slab effects. J Cons Steel Res 2012;68(1):165-75.

[4] Nie JG, Tao MX. Slab spatial composite effect in composite frame systems. I: Effective width for ultimate loading capacity. Eng Struct 2012;38:171-84.

[5] Fang J, Bao W, Ren F, Pang L, Jiang J. Behaviour of composite beams with beam-to-girder end-plate connection under hogging moments. Eng Struct 2021;235(5):112030.

[6] Lin W, Yoda T, Taniguchi N, Kasano H, He J, Mechanical performance of steel-concrete composite beams subjected to a hogging moment. J Struct Eng 2013;140(1):04013031.

[7] Li VC, Leung CKY. Steady-state and multiple cracking of short random fiber composites. J Eng Mech 1992;118:2246-64.

[8] Li V C. Engineered Cementitious Composites (ECC) –material, structural and durability performance. In: E. Nawy (Ed.), Concrete Construction Engineering Handbook (2nd ed.), Boca Raton: CRC Press, 2009, Chapter 24.

[9] Singh M, Saini B, Chalak H D. Performance and composition analysis of engineered cementitious composite (ECC) – A review. J Build Eng 2019; 26:100851.

[10] Li RZ, Deng MK, Zhang YX, Wei D. Shear strengthening of reinforced concrete deep beams with highly ductile fiber-reinforced concrete jacket. J Build Eng,2021;48: 103957

[11] Wang ZB, Wang PY, Zhu FQ. Synergy effect of hybrid steel-polyvinyl alcohol fibers in engineered cementitious composites: Fiber distribution and mechanical performance. J Build Eng, 2022;62:105348

[12] Fan JS, Gou SK, Ding R, Zhang J, Shi ZJ. Experimental and analytical research on the flexural behaviour of steel-ECC composite beams under negative bending moments. Eng Struct 2020;210:17.

[13] Rana MM, Lee CK, Al-Deen S, Zhang YX. Flexural behaviour of steel composite beams encased by engineered cementitious composites. J Constr Steel Res 2018;143:279.

[14] Khan M, Lee C K, Zhang Y X. Parametric study on high strength ECC-CES Composite Columns under Axial Compression. J Build Eng, 2021;8:102883.

[15] Yang X, Xu L, Pan JL. Mechanical behavior of full-scale composite steel plate shear wall restrained by ECC panels. J Build Eng, 2021;44:102864.

[16] Nie X, Duan LL, Zhuang LD, Ding R, Fan JS. Experimental and numerical study on steel-concrete composite frames with engineered cementitious composites. Eng Struct 2022;265:114489.

[17] Nie JG, Wang JG, Gou SK, Zhu YY, Fan JS. Technological development and engineering applications of novel steel-concrete composite structures. Front Struct Civ Eng 2019;13(1):1-14.

[18] Nie X, Fan JS, Shi YJ. Elastic analysis of composite beam with local-released combined action. China Civil Eng J 2013;46(11):105-111.(in Chinese).

[19] Duan LL, Chen HB, Nie X, Han SW. Experimental study on steel-concrete composite beams with Uplift-restricted and slip-permitted screw-type (URSP-S) connectors. Steel Compos Struct 2020;35(2):261-78.

[20] Zhu L, Wang JJ, Li X, Tang L, Yu BY. Experimental and numerical study of curved SFRC and ECC composite beams with various connectors. Thin Wall Struct 2020;155:106938.

[21] Nie X, Duan LL, Tao MX, Guo YT. Experimental investigation on the behavior of the steel-concrete composite frames with uplift-restricted and slip-permitted screw-type (URSP-S) connectors. Eng Struct

2022;254:113868.

[22] Duan L, Nie X, Ding R, Zhuang L. Research on application of uplift-restricted slip-permitted (URSP) connectors in steel-concrete composite frames Appl Sci. 2019;9(11):2235.

[23] Li ZY, Tao MX, Nie JG, Fan JS. Analysis and optimization of a continuous composite bridge with uplift-restricted and slip-permitted connectors. In IABSE Symposium Report; International Association for Bridge and Structural Engineering: Zurich, Switzerland, 2017.

[24] MSC. Software Corp. MSC. Marc user's manual. MSC. Software Corporation, Santa Ana, CA; 2007.

[25] JGJ 138-2016. Code for Design of Composite Structures. Beijing, China: China Architecture & 468 Building Press; 2016. (in Chinese).

[26] GB 50011-2010. Code for Seismic Design of Buildings. Beijing, China: China Architecture & Building Press; 2010. (in Chinese).

[27] GB/T 50081-2019， Standard for Test Methods of Concrete Physical and Mechanical Properties Ministry of housing and urban-rural development of China, Beijing, China (2019). (in Chinese).

[28] Gou SK, Ding R, Fan JS, Nie X, J. Zhang, Experimental study on seismic performance of precast LSECC/RC composite joints with U-shaped LSECC beam shells. Eng Struct 2019;189(JUN.15):618-34.

[29] GB/T228-2010. Metallic Materials-Tensile Testing at Ambient Temperature. Beijing, China: China Standards Press; 2010. (in Chinese).

[30] GB 50009-2012. Load code for the design of building structures. Beijing, China: China Architecture & Building Press; 2012. (in Chinese).

[31] Peng P, Gang Z, Lu X, Deng K. Force-displacement mixed control for collapse tests of multistory buildings using quasi-static loading systems. Earthquake. Eng Struct 2014;43(2):287–300.

[32] Wang JJ, Tao MX, Zhou M, Nie X. Force transfer mechanism in RC beams strengthened in shear by means of steel plated concrete. Eng Struct 2018;171:56-71.

[33] Amadio C , Bedon C , Fasan M , Pecce MR. Refined numerical modelling for the structural assessment of steel-concrete composite beam-to-column joints under seismic loads. Eng Struct 2017;138:394-409.

[34] Braconi A, Bursi OS, Fabbrocino G, Salvatore W, Tremblay R. Seismic performance of a 3D full-scale high-ductility steel–concrete composite moment-resisting structure— Part II: test results and analytical validation. Earthq Eng Struct Dyn 2008;37:1635-1655.

[35] Bursi OS, Sun FF. Non-linear analysis of steel–concrete composite frames with full and partial shear connection subjected to seismic loads. J Constr Steel Res 2005;61(1):67-92.

[36] Zhou F, Mosalam KM, Nakashima M. Finite-element analysis of a composite frame under large lateral cyclic loading. J Struct Eng 2007;133(7):1018-1026.

[37] Rüsch H. Research toward a general flexural theory for structural concrete. ACI Struct J 1960;July:1-28

[38] Huang T, Zhang XY. Numerical modelling of mechanical behaviour of engineered cementitious composites under axial tension. Comput Struct 2016;173:95-108.

[39] Wang W, Teng S. Finite-element analysis of reinforced concrete flat plate structures by layered shell element. J Struct Eng 2008;134:1862-72.

[40] Ollgaard JG., Slutter RG Fishe JW. Shear strength of stud connectors in lightweight and normal-weight concrete. AISC Eng J Am Inst Steel Constr 1971;169(8):55-64.

[41] Amadio C , Bedon C , Fasan M. Numerical assessment of slab-interaction effects on the behaviour of steel-concrete composite joints. J Constr Steel Res 2017;139:397-410.